# **Inorganic Chemistry**

pubs.acs.org/IC Article

# Electronic Structures of Cr(III) and V(II) Polypyridyl Systems: Undertones in an Isoelectronic Analogy

Justin P. Joyce,<sup>†</sup> Romeo I. Portillo,<sup>†</sup> Collette M. Nite, Jacob M. Nite, Michael P. Nguyen, Anthony K. Rappé,\* and Matthew P. Shores\*



Cite This: Inorg. Chem. 2021, 60, 12823-12834



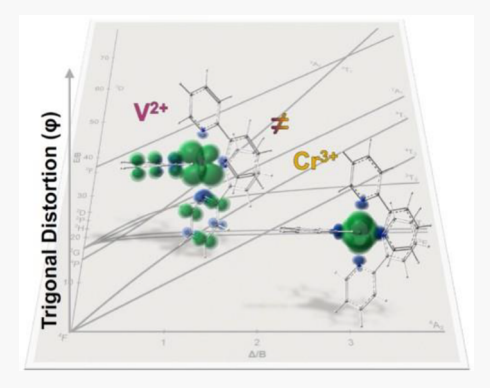
**ACCESS** 

Metrics & More

Article Recommendations

Supporting Information

**ABSTRACT:** A recently reported description of the photophysical properties of  $V^{2+}$  polypyridyl systems has highlighted several distinctions between isoelectronic,  $d^3$ ,  $Cr^{3+}$ , and  $V^{2+}$  tris-homoleptic polypyridyl complexes of 2,2'-bipyridine (bpy) and 1,10-phenanthroline (phen). Here, we combine theory and experimental data to elucidate the differences in electronic structures. We provide the first crystallographic structures of the  $V^{2+}$  complexes  $[V(bpy)_3](BPh_4)_2$  (V-1B) and  $[V(phen)_3](OTf)_2$  (V2) and observe pronounced trigonal distortion relative to analogous  $Cr^{3+}$  complexes. We use electronic absorption spectroscopy in tandem with TD-DFT computations to assign metal—ligand charge transfer (MLCT) properties of V-1B and V2 that are unique from the intraligand transitions,  $^4(^3IL)$ , solely observed in  $Cr^{3+}$  analogues. Our newly developed natural transition spin density  $(NT\rho^{\alpha,\beta})$  plots characterize both the  $Cr^{3+}$  and  $V^{2+}$  absorbance properties. A multideterminant approach to DFT assigns the energy of the  $^2E$  state of V-1B as stabilized through



electron delocalization. We find that the profound differences in excited state lifetimes for  $Cr^{3+}$  and  $V^{2+}$  polypyridyls arise from differences in the characters of their lowest doublet states and pathways for intersystem crossing, both of which stem from trigonal structural distortion and metal–ligand  $\pi$ -covalency.

# **■ INTRODUCTION**

Octahedral Cr3+ complexes have received intense research interest due to their attractive photophysical properties and the relative natural abundance of chromium. 1,2 The interpretation of their absorption spectra was foundational in the advancement of both crystal and ligand field theories, and the spectra themselves provide critical benchmarks for computational methods.3-6 The long-lived excited state of Cr3+ complexes is attributed to the minimal geometric distortion and hence minimal nonradiative decay associated with the spin-flip nature of the low-lying  ${}^{2}E$  state (using  $O_{h}$  symmetry notation). Because the energy of the <sup>2</sup>E state for Cr<sup>3+</sup> is approximately independent of ligand field, being dominantly impacted by interelectronic repulsion, it is anticipated that slow emission is an innate property of  $d^3$  systems, and this attribute should transfer to the isoelectronic  $V^{2+}$  analogues—but it does not.8-10 Thus, elucidating a more nuanced understanding of the electronic properties of d<sup>3</sup> polypyridyls is essential for the hopeful application of these coordination complexes in photovoltaic devices and photocatalytic processes.

Herzog and König reported the initial comparison of  $[V(bpy)_3]^{2+}$  and  $[Cr(bpy)_3]^{3+}$  in 1970. Their analysis treated  $V^{2+}$  and  $Cr^{3+}$  absorbances interchangeably in the context of ligand field transitions. This isoelectronic analogy was strained by inconsistencies with respect to the magnitude of molar absorptivities, relative ligand field strengths (10 Dq),

and metal-centered exchange interaction energies (B). Findings by Maverick and co-workers in the late 1980s further shook the equivalency of these isoelectronic species when they reported that  $[V(bpy)_3]^{2+}$  has an excited state lifetime of 0.5 ns, which pales in comparison to the 400  $\mu$ s lifetime of its Cr<sup>3+</sup> analogue. <sup>13,14</sup> While <sup>2</sup>E states of V<sup>2+</sup> polypyridyl complexes evade a precise energetic assignment, Dill et al. recently refined our understanding of these species through a detailed spectroscopic study and characterization of the role of charge transfer in their excited state manifold. <sup>15</sup>

Herein, we focus on the distinctions between the geometric and electronic structures of the ground and excited states of isoelectronic  $Cr^{3+}$  and  $V^{2+}$  polypyridyl systems to discern the source(s) of their divergent physicochemical properties. The paper is organized as follows. First, we disclose novel crystallographic analyses of the first  $V^{2+}$  polypyridyl systems and compare their structures with analogous  $Cr^{3+}$  systems from the literature; we characterize the trigonal distortion of the  $V^{2+}$  complexes using the continuous shape measurement (CShM)

Received: April 12, 2021 Published: August 12, 2021





Second, we present a multireference electronic structure description, including spin—orbit coupling, for the manifold of metal-centered excited states for a small model complex. Third, we use DFT computations to analyze the electronic structures of the metal and ligand orbitals of both  $V^{2+}$  and  $Cr^{3+}$  polypyridyl complexes. Fourth, we assign the experimentally observed visible-light absorbance of  $V^{2+}$  and  $Cr^{3+}$  polypyridyls using TD-DFT and illustrate changes with a newly developed density display procedure. Finally, we assign the low-lying doublet excited states of  $Cr^{3+}$  and  $V^{2+}$  polypyridyl complexes.

### RESULTS AND DISCUSSION

Geometric Structural Analyses. Six-coordinate d<sup>3</sup> metal complexes are anticipated to have well-defined near-octahedral geometries due to an isotropic electronic configuration and large ligand field stabilization energy. The Cambridge Crystallographic Structural Database (CCSD) reports 22  $Cr^{3+}$  polypyridyl complexes that we refer to as  $[Cr(NN)_3]^{3+}$  16 The average Cr-N distance in this set is 2.048(7) Å, equivalent to a factor of 0.975(3) when scaled with respect to the sum of their covalent radii,  $R\sum_{cov} r_{cov}^{-1.17,18}$  The octahedral coordination environment is quantified with the continuous shape measure (CShM) approach. This procedure assigns the angular distortional distance between the experimental structure and a reference polyhedra, providing a quantitative assessment of a metal center's coordination geometry. We report a small average value of 0.779, where deviation from zero indicates geometric distortion. 19 Of interest is that the Cr3+ complexes closely reside at one end of the distortion pathway between octahedral (OC-6) and trigonal prismatic (TRP-6) geometries, ~21% ( $\varphi_{OC \rightarrow TRP}$ ), a distortion known as a Bailar twist.<sup>20</sup>

We introduce the first crystallographic characterizations of  $V^{2+}$  polypyridyl complexes. The  $V^{2+}$  complex in  $[V(bpy)_3]$ -(BPh<sub>4</sub>)<sub>2</sub> (V-1B) has an average V-N bond distance of 2.133(5) Å that is contracted relative to the  $[Cr^{3+}(NN)_3]$ structures when scaled with respect to their covalent radii, 0.952(1)  $R\sum r_{cov}^{-1}$ . Meanwhile,  $[V(phen)_3](OTf)_2$  (V2) possesses a very similar average V–N bond length of 2.177(8) Å with a sum of covalent radii equal to 0.951(2)  $R\sum_{r_{cov}}^{-1}$  (see the Supporting Information). We equate the contracted bond length in vanadium analogues with greater metal-ligand covalency, consistent with greater nuclear shielding and larger size of the 3d orbitals of V<sup>2+</sup>. V1b has an OC-6 measure of 1.82 which is associated with a  $\varphi_{\text{OC}\to\text{TRP}}$ of 32.1%. The largest Bailar twist conversion reported for a trisbidentate d<sup>3</sup> system is 38%, highlighting the significant magnitude of the structural distortion of V-1B.21 A similar, though less pronounced, distortion is observed for V2 with an S(OC-6) of 1.20 and a  $\varphi_{\text{OC} \rightarrow \text{TRP}}$  of 26.6%. Their crystal structures are presented alongside their minimal distortion pathway in Figure 1, indicating that  $V^{2+}$  polypyridyls possess greater trigonal distortion than their  $Cr^{3+}$  analogues.

Electronic Structural Analyses. Excited State Surface Crossing for ISC. The isoelectronic  $V^{2+}$  and  $Cr^{3+}$  free ions have  ${}^4F$  ground states and low-lying  ${}^2G$  excited states with experimental J-averaged excitation energies of 1.46 eV (11800 cm $^{-1}$ ) and 1.82 eV (14700 cm $^{-1}$ ), respectively. $^{22}$  In an octahedral environment, the 9-fold degenerate  ${}^2G$  state splits into  ${}^2E$ ,  ${}^2T_2$ ,  ${}^2T_1$ , and  ${}^2A$  states; see the Tanabe–Sugano diagram in Figure 2. Emission is not observed for  $[V(bpy)_3]^{2+}$ , while for  $[Cr(bpy)_3]^{3+}$  emission from the  ${}^2E$  excited state occurs at 1.78 eV (14300 cm $^{-1}$ ). $^{15,23}$  Computationally, the

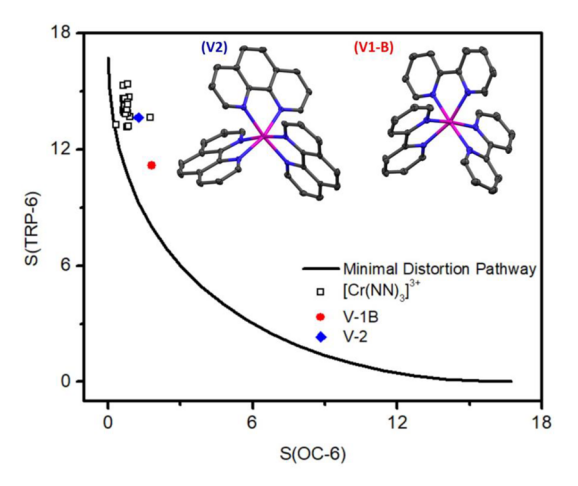
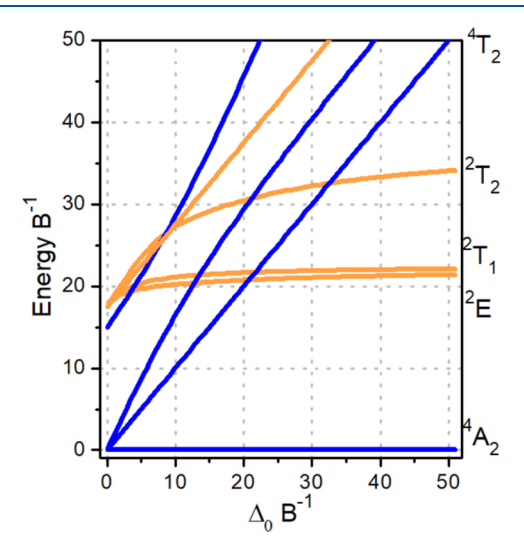


Figure 1. Continuous shape measure (CShM) correlation between trigonal prismatic (TPR-6) and octahedral (OC-6) geometries (solid line) for the  $[Cr(NN)_3]^{3+}$  data set (open black squares) and our reported structures for V-1B (red circle) and V2 (blue diamond). Crystal structures for the cationic complexes in V-1B and V2 are shown in the inset, where hydrogen atoms, anions, and cocrystallized solvent molecules are omitted for clarity. Thermal ellipsoids are set to 40%.



**Figure 2.** Simplified Tanabe–Sugano diagram for a  $d^3$  transition metal center in an  $O_h$  coordination where blue and orange denote a quartet and doublet state, respectively.

 $[V(bpy)_3]^{2+}$   $^2E$  state is reported to range between 0.9 eV (7300 cm  $^{-1}$ ) and 1.16 eV (9360 cm  $^{-1}$ ), while comparable methods place the  $^2E$   $[Cr^{3+}(bpy)_3]$  at 1.6 eV (13000 cm  $^{-1}$ ).  $^{15}$ 

Nonobservation of emission could be due to either a lack of formation of the emissive excited state or a rapid nonradiative decay of the emissive excited state. Excitation of the  $^4\mathrm{A}_2$  ground state to the  $^4\mathrm{T}_2$  excited state  $(t_{2g}^2-e_g^{*1})$  can result in geometric distortion that can provide a mechanism for intersystem crossing (ISC) to the doublet manifold. As discussed above, for a  $d^3$  system, in an octahedral or a near-octahedral field there are nine potentially low-lying metal-centered doublet states, most of which are multiconfigurational and hence are not accessible to TD-DFT. To examine the distortion hypothesis, we use a multiconfigurational spectroscopy oriented configuration interaction (SORCI) method  $^{24}$  to provide a balanced description of the full manifold of low-lying

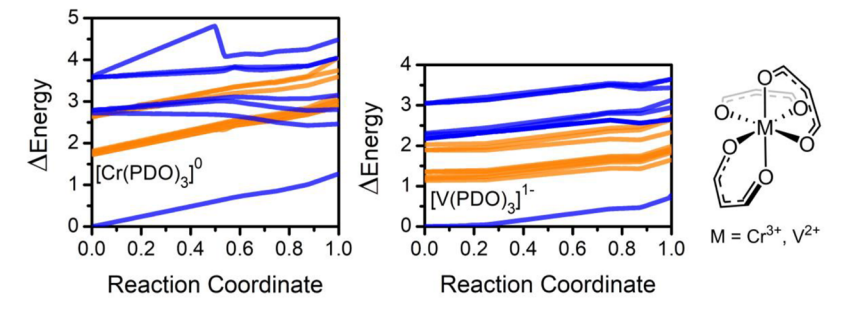
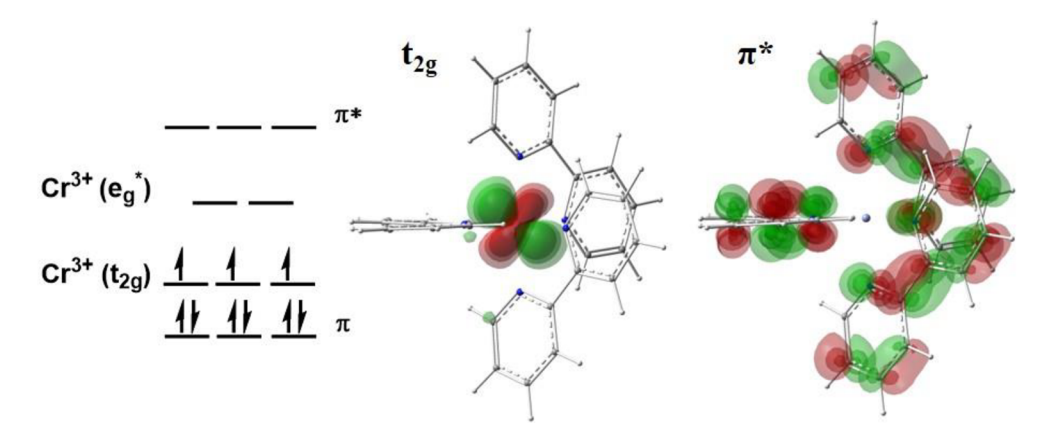


Figure 3. Plots of metal-centered excited states of  $[Cr^{3+}(PDO)_3]$  (left) and  $[V^{2+}(PDO)_3]^-$  (middle) along a linear distortion reaction coordinate between the  $^4A_{2g}$  and  $^4T_{2g}$  optimized geometries that are defined as 0 and 1, respectively. The blue and orange lines represent the quartet and doublet states, respectively. Right: structure of the model  $[M(PDO)_3]^n$  complexes.



**Figure 4.** (left) Qualitative orbital diagram for  $[Cr(bpy)_3]^{3+}$  where the vertical axis is energy. (right) Representative orbitals of the triply degenerate  $t_{2g}$  and  $\pi^*$ -orbitals of  $[Cr(bpy)_3]^{3+}$ .

metal-centered excited states along the TD-DFT-based structural distortion pathway between the <sup>4</sup>A<sub>2</sub> and <sup>4</sup>T<sub>1</sub> states. The significant increase in computational resource utilization for SORCI led us to study the model complexes  $[Cr(PDO)_3]$ and  $[V(PDO)_3]^-$ , where PDO = 1,3-propanedionato, which is further detailed in the Supporting Information.<sup>25</sup> PDO provides a 3-fold symmetric ligand field with a modest  $\pi$ system. The overall charge of the model complexes is 0 and -1for the Cr3+ and V2+ species, respectively. The active space utilized three electrons and five d orbitals. Inclusion of spinorbit coupling results in significant mixing between the doublet and quartet state manifolds in [Cr(PDO)<sub>3</sub>] (see Figure 3). These findings are consistent with previous studies on the related complex,  $[Cr(acac)_3]^{26-28}$  In contrast, a crossing point is not observed between the excited quartet and metal-centered doublet state manifolds of the corresponding V<sup>2+</sup> complex. The lowered energy of the doublet manifold for V<sup>2+</sup> relative to Cr<sup>3+</sup> provides this energetic separation. Thus, intersystem crossing to the doublet manifold in V2+ complexes via geometric distortion via the  ${}^4T_2 \leftarrow {}^4A_2$  transition is not likely without significant ligand  $\pi$ -system intervention.

 $M(bpy)_3$  Structural Distortion. Further computational discussion is centered on  $[Cr(bpy)_3]^{3+}$  and  $[V(bpy)_3]^{2+}$  complexes, where DFT calculations were performed with the APFD hybrid-DFT functional that we have previously used for the analysis of  $Cr^{3+}$  and  $V^{2+}$  octahedral complexes. Sp. We note that the S(OC-6) values of the optimized structures are in quantitative agreement with the experimental structures discussed above. The 3d orbitals of the  $Cr^{3+}$  complex display the classic  $t_{2g}-e_g^*$  ligand field splitting anticipated for a near-octahedral coordination environment—despite the ligand-

imposed reduction in symmetry to  $D_3$  that is shown in Figure 4.

Although it is commonly classified as a  $\pi^*$ -acceptor, we emphasize here that bipyridine is poised as a  $\pi$ -donor with respect to the  $Cr^{3+}$  metal center, in agreement with the angular overlap model (AOM) that assigns ligand field properties, such as  $\sigma$ - and  $\pi$ -bonding ability, based on the orbital overlap between a metal center and its ligands. It has previously been reported that for  $Cr^{3+}$  complexes bipyridine is a weakerfield ligand in the spectrochemical series than ethylenediamine, a ligand of pure  $\sigma$ -character. This distinction is important since increasing the ligand field strength of  $Cr^{3+}$  octahedral complexes represents an effective strategy to inhibit backintersystem crossing to maximize excited state lifetimes.

In agreement with the crystal structure for V1b, there is a reduction in symmetry from  $O_h$  to  $D_3$  for the computed structure for [V(bpy)<sub>3</sub>]<sup>2+</sup> that alleviates the 3-fold degeneracy of the  $t_{2g}$  set into  $a_1$  + e sets. The e orbitals engage in both donor and acceptor interactions with the  $\pi$ - and  $\pi^*$ -orbitals of the polypyridyl ligand set. The metal-centered e orbitals are destabilized relative to the a1 orbital and are in a predominantly nonbonding arrangement with the bipyridyl  $\pi$ -system, we refer to this pair as  $e_{\delta}$ . The complementary ligand e set is stabilized upon structural distortion—providing the electronic basis for the structural distortion. Analogous bonding properties of bipyridine have been recently reported for low-spin Fe<sup>2+</sup> complexes.<sup>38,39</sup> Our findings are complementary to an earlier report by Dobson and Taube indicating that  $V^{2+}$  polypyridyls possess minimal  $\pi^*$ -backbonding despite the sensitivity of their reduction potential to ligand identity. 40

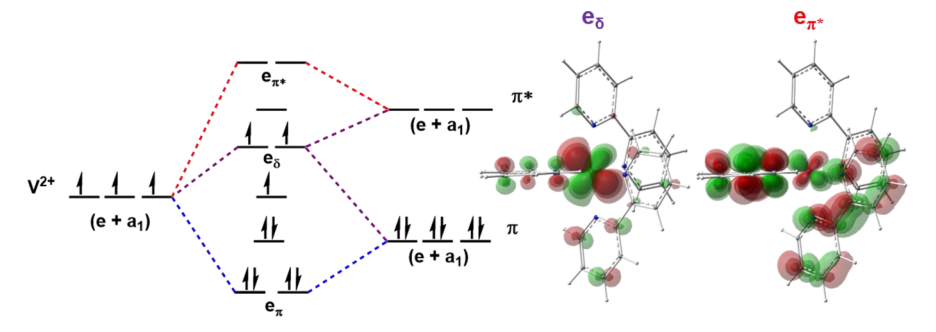


Figure 5. (left) Qualitative orbital diagram for  $[V(bpy)_3]^{2+}$  where the vertical axis is energy; the  $V^{2+}$  " $e_g$ " orbitals are omitted from the diagram. (right) Representative orbitals of the doubly degenerate  $e_\delta$  and  $e_{\pi^*}$  orbitals of  $[V(bpy)_3]^{2+}$ .

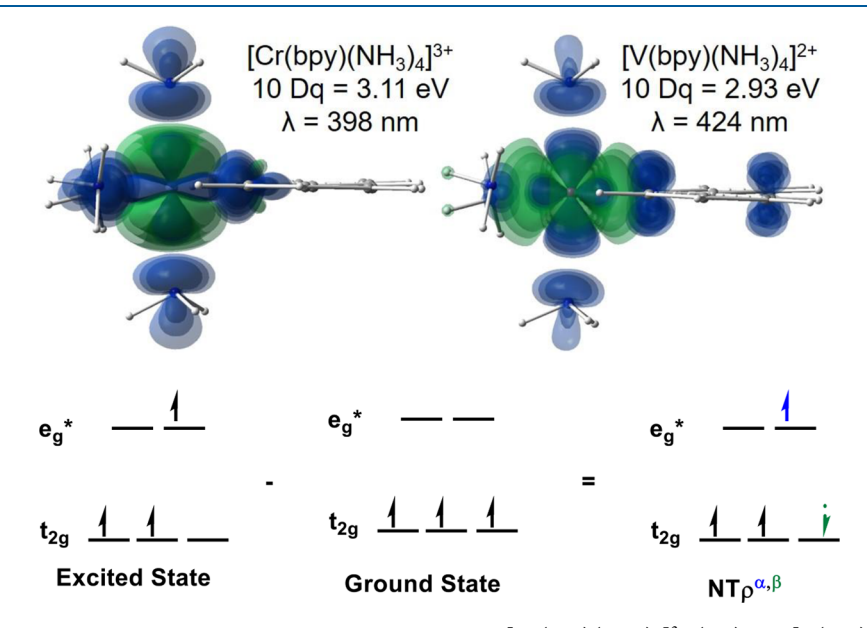


Figure 6. (top) NT $\rho^{\alpha,\beta}$  plots, described below, of the ligand field transitions for  $[Cr(bpy)(NH_3)_4]^{3+}$  (left) and  $[V(bpy)(NH_3)_4]^{2+}$ . Green denotes the loss of α-electron density in the ground state. Blue represents the increase of α-electron density in the excited state (right). Their ligand field strength (10 Dq) and wavelength (λ) computed from TD-DFT are provided. (bottom) Their associated qualitative orbital energy diagrams are presented below with respect to  $O_h$  symmetry.

The associated qualitative orbital diagram and pertinent orbitals for  $[V(bpy)_3]^{2+}$  are presented in Figure 5. Collectively, these electronic structure properties corroborate the trigonal distortion that is observed crystallographically for  $[V(bpy)_3]^{2+}$  relative to  $[Cr(bpy)_3]^{3+}$ . As discussed below, the higher lying/larger d orbitals of  $V^{2+}$  provide greater covalency to the interactions with the bipyridyl ligands. While geometric and electronic structures are inseparable, we maintain that the  $\pi$ -interactions described above predicate the trigonal distortion of the complex.

Figure 6 presents natural transition spin density  $(NT\rho^{\alpha,\beta})$  plots for the lowest metal-based quartet excitations of  $[Cr(NH_3)_4(bpy)]^{3+}$  and  $[V(NH_3)_4(bpy)]^{2+}$ . The model complexes displayed in Figure 6 are provided strictly for visual clarity, and we note that their transition energies and characters are interchangeable with the corresponding trisbidentate polypyridyl complexes. In these plots, the TD-DFT calculated  $\alpha$  and  $\beta$  spin densities of an excited state are subtracted from the respective spin densities of its ground state. Blue denotes a positive value that is attributed to an increase of  $\alpha$ -electron density in the excited state or a decrease of  $\beta$ -electron density in the ground state. Green is the negative value associated with an increase of  $\beta$ -electron density in the

excited state or loss of  $\alpha$ -electron density in the ground state. The NT $\rho^{\alpha,\beta}$  plots in Figure 5 illustrate the archetypal  $e_g^* \leftarrow t_{2g}$  d–d ligand field processes. We note that the NT $\rho^{\alpha,\beta}$  plot of  $[V(bpy)(NH_3)_4]^{2+}$  shows greater metal–ligand covalency, descriptive of the nephelauxetic effect, and significant ligand  $\pi$ -character that will be detailed further below.

**Intraligand Excitation.** The NT $\rho^{\alpha,\beta}$  plots associated with near-UV ( $\lambda_{max}$  = 307 nm) and visible light ( $\lambda_{max}$  = 425 nm) absorbance of  $[Cr(bpy)(NH_3)_4]^{3+}$  are presented in Figure 7. Both transitions display dominantly ligand character with complementary relative spin densities. The visible light absorbance has been previously assigned as an intraligand,  $\pi^* \leftarrow \pi$ , transition at lower energy than the intraligand singlet transition <sup>4</sup>(<sup>1</sup>IL). <sup>41</sup> This suggests that the visible-light absorbance is associated with a triplet excitation of the coordinated bipyridine, <sup>4</sup>(<sup>3</sup>IL). Despite extensive characterization, the visible light absorbance of Cr3+ continues to evade a definite classification. 42,43 The 4(3IL) description of the electronic absorbance of Cr3+ polypyridyls was originally offered by Ohno et al. upon discounting its assignment as a ligand field transition. 44 Herein, we provide a computational characterization of the <sup>4</sup>(<sup>3</sup>IL). We note that the transition at

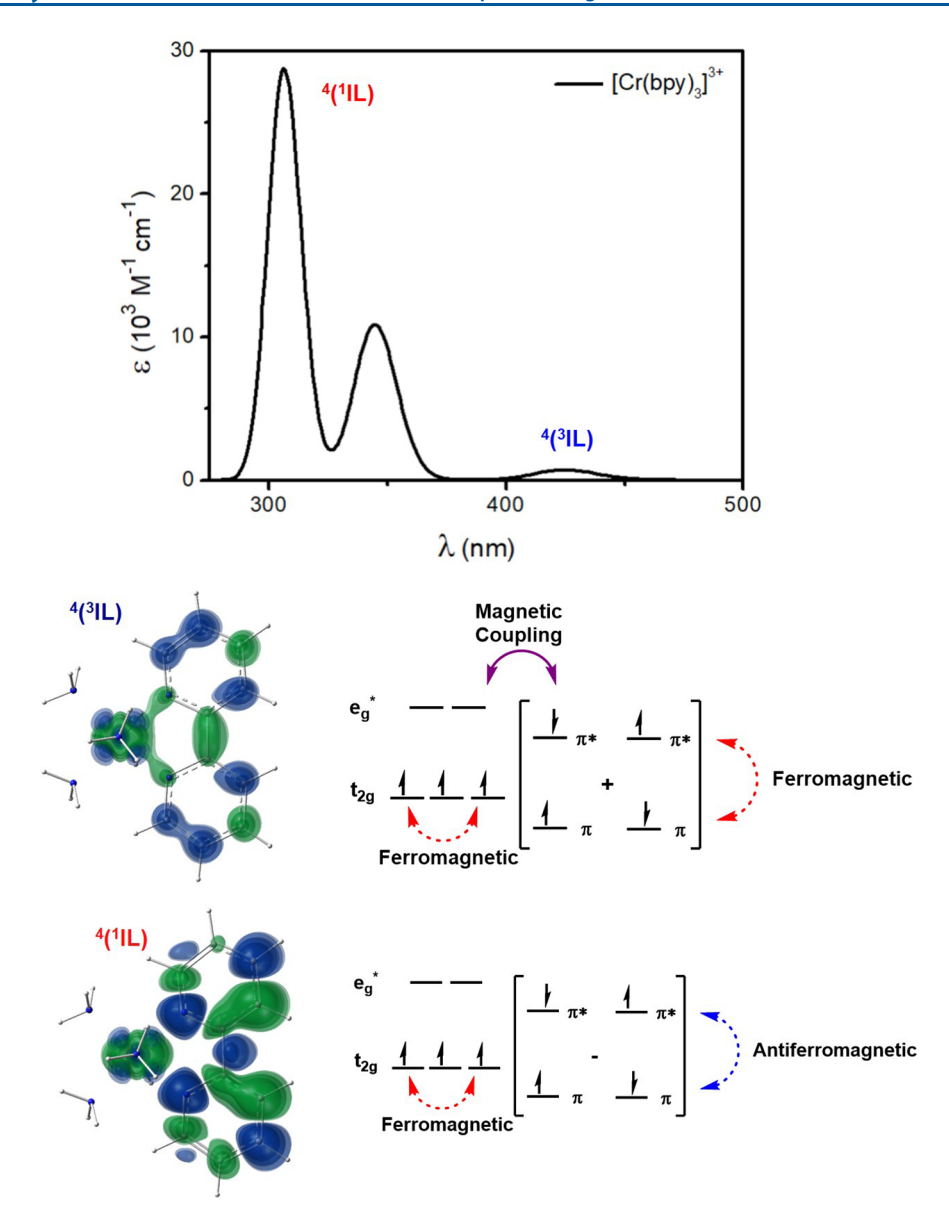


**Figure 7.** Electronic absorbance spectrum of  $[Cr(bpy)_3]^{3+}$  as calculated by TD-DFT. For clarity, the  $NT\rho^{\alpha,\beta}$  are shown with the corresponding transition of  $[Cr(bpy)(NH_3)_4]^{3+}$ . The orbital diagrams provided below offer a multideterminant representation of the labeled transitions.

 $\lambda_{\rm max}$  = 355 nm is a ligand-to-metal charge transfer (LMCT), and its corresponding NT $\rho^{\alpha,\beta}$  is included in Figure S13.

The two-electron spin eigenfunctions of the bipyridine triplet and singlet electronic configurations in terms of  $\alpha$  and  $\beta$ spins are provided in eqs 1-4 and correspond to the ligand excited state. Spin eigenfunctions are combinations of individual electron spin determinants that form proper S and  $M_{\rm s}$  representations. The ligand triplet states exhibit magnetic exchange interactions with the paramagnetic metal center (see eqs 5-8 for the quartet spin eigenfunctions) to yield a Heisenberg-Dirac-van Vleck (HDvV) spin ladder of sextet, quartet, and doublet states. The sextet and doublet states can be thought of as parallel (ferromagnetic) and antiparallel (antiferromagnetic) coupling between a metal-centered quartet pseudospin and a ligand-centered triplet pseudospin. If the doublet HDvV state is lowest in energy, it is said that there is antiferromagnetic coupling, while if the sextet state is lowest in energy, the system is said to be ferromagnetically coupled. While the sextet can be described with a single determinant, as

described in the Supporting Information, a proper description of the doublet state requires 10 spin determinants—in DFT this is approximated a simple broken symmetry model of indeterminant spin.  $^{45,46}$  The intermediate quartet state (neither ferro- nor antiferromagnetically coupled) is associated with the observed 425 nm transition whose dominant five-spin determinant representation is provided in eq 11, illustrated in Figure 7, and tabulated in the Supporting Information. It consists of the negative combination of the  $M_{\rm s}=0$  triplet spin eigenfunction of the ligand and  $M_{\rm s}=3/2$  metal-centered quartet state with the  $M_{\rm s}=1/2$  metal-centered quartet spin eigenfunction and the  $M_{\rm s}=1$  triplet spin eigenfunction of the ligand. The multireference N-electron valence state perturbation theory NEVPT2(5,7) method is used  $^{47-49}$  to compute the spin energetics and analysis.

$$(\alpha \alpha)$$
 ligand-based triplet:  $M_s = 1$  (1)

$$(\alpha\beta + \beta\alpha)$$
 ligand-based triplet:  $M_s = 0$  (2)

$$(ββ)$$
 ligand-based triplet:  $M_s = -1$  (3)

$$(\alpha\beta - \beta\alpha)$$
 ligand-based singlet:  $M_s = 0$  (4)

$$(\alpha \alpha \alpha)$$
 metal-centered quartet:  $M_s = 3/2$  (5)

$$\frac{1}{\sqrt{3}}(\alpha\alpha\beta + \alpha\beta\alpha + \beta\alpha\alpha) \text{ metal-based quartet: } M_{\rm s} = 1/2$$
 (6)

$$\frac{1}{\sqrt{3}}(\beta\beta\alpha + \beta\alpha\beta + \alpha\beta\beta) \text{ metal-based quartet: } M_{\rm s} = -1/2$$
 (7)

$$(βββ)$$
 metal-centered quartet:  $M_s = -3/2$  (8)

$$\frac{1}{\sqrt{2}}(\alpha\beta\alpha - \beta\alpha\alpha) \text{ metal-based doublet: } M_{\rm s} = 1/2 \tag{9}$$

$$\frac{1}{\sqrt{6}}(2\alpha\alpha\beta - \alpha\beta\alpha - \beta\alpha\alpha) \text{ metal-based doublet: } M_{\rm s} = 1/2$$
(10)

$$(\alpha\beta + \beta\alpha)(\alpha\alpha\alpha) - (\alpha\alpha)(\alpha\alpha\beta + \alpha\beta\alpha + \beta\alpha\alpha)^{4}(^{3}IL)$$
(11)

$$(\alpha\beta - \beta\alpha)(\alpha\alpha\alpha)^{4}(^{1}IL)$$
 (12)

The intermediate coupling of the ligand triplet to the unpaired electrons on the metal center provides a mechanism for the spin-forbidden triplet excitation to have intensity. The <sup>4</sup>(<sup>3</sup>IL) excitation in the experimental electronic absorption spectrum of  $[Cr(bpy)_3]^{3+}$  exhibits features that are resolved by ~520 cm<sup>-1</sup>, suggested to correspond to the C<sub>py</sub>-C<sub>py</sub> stretching modes of the cis-conformation of bipyridine. Optimization of the excited state geometry and inclusion of vibronic coupling between the ground and lowest-lying quartet excited state lead to a computed spectrum that displays this vibrational feature. In addition, projecting the excited state structural distortion onto the vibrational modes supports the  $C_{py}-C_{py}$  stretching mode assignment. These results are further detailed in the Supporting Information. In addition to providing an absorption pathway, modest spin-orbit coupling between the states of the Heisenberg spin ladder provides a viable pathway for the 4(3IL) excited state to undergo intersystem crossing (ISC) to the potential energy surface of the associated doublet state for Cr<sup>3+</sup>. The coupling constant between the paramagnetic metal center and ligand triplet excited state was calculated with a HDvV model Hamiltonian that simplifies to the following equation for a two-center interaction where  $S_1$ and  $S_2$  refer to the proper  $M_s$  of spin center one and two, respectively:

$$J = \frac{E(S_1) - E(S_2)}{S_1(S_1 + 1) - S_2(S_2 + 1)}$$
(13)

Spin center one has the larger spin value so that positive and negative coupling values refer to ferro- and antiferromagnetic exchange interactions, respectively. NEVPT2(5,7) classifies the  ${}^{4}({}^{3}\text{LL})$  of  $[\text{Cr(bpy)}(\text{NH}_{3})_{4}]^{3+}$  as an antiferromagnetic interaction with J=-126 cm<sup>-1</sup>. We also report the presence of a  ${}^{4}({}^{3}\text{LL})$  transition in  $[\text{V(bpy)}(\text{NH}_{3})_{4}]^{2+}$  which has a smaller antiferromagnetic coupling  $(J=-75.3 \text{ cm}^{-1})$  and is red-shifted with respect to its  $\text{Cr}^{3+}$  analogue. We note that this model does not distinguish the competing ferro- and antiferromagnetic

interactions that define the  ${}^4({}^3\mathrm{IL})$  state which is illustrated in Figure 7.

**MLCT Transitions.** As described above, electronic absorbance spectra of  $V^{2+}$  polypyridyl complexes show significant absorbance in the visible region that are associated with a metal-to-ligand charge transfer transition (MLCT) at  $\lambda_{max}$  of 643 nm, whereas similar events for  $Cr^{3+}$  are not observed. The experimental absorbance spectra of the  $Cr^{3+}$  and  $V^{2+}$  polypyridyl complexes are provided in Figure 8. The

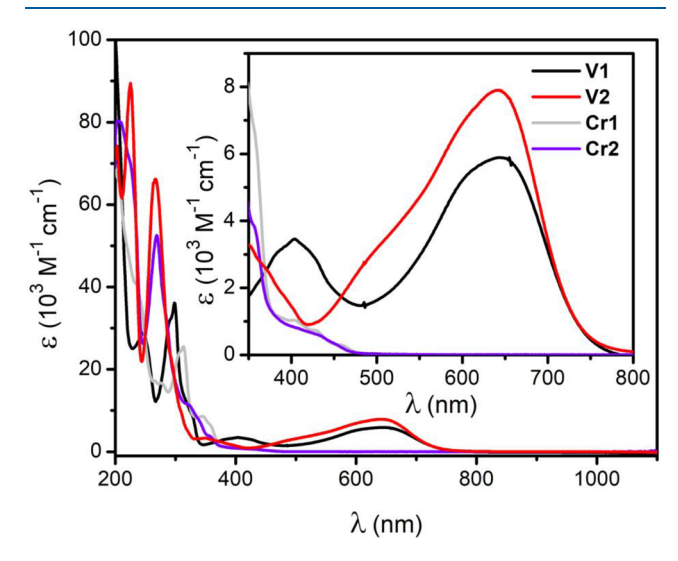
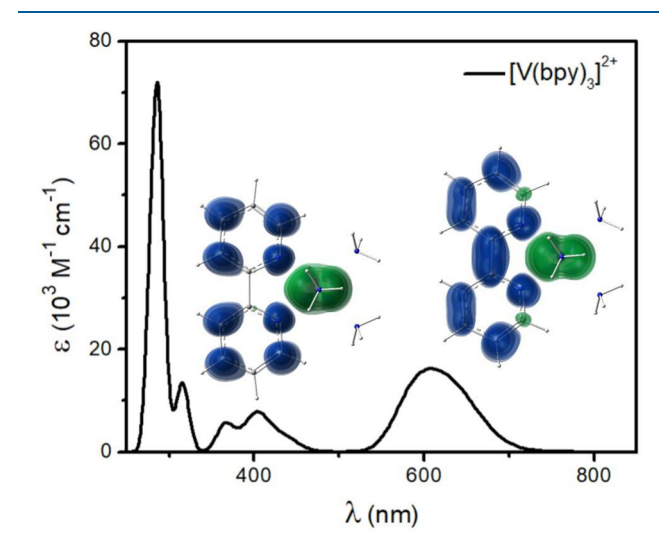


Figure 8. Electronic absorption spectra of  $[V(bpy)_3(OTf)_2]$  (V; black),  $[V(phen)_3(OTf)_2]$  (V2; red),  $[Cr(bpy)_3](BF_4)_3$  (Cr1; gray), and  $[Cr(phen)_3](BF_4)_3$  (Cr2; purple) collected in CH<sub>3</sub>CN.

NT $\rho^{\alpha,\beta}$  plot shown in Figure 9 provides an unambiguous description as a  $\pi^* \leftarrow e_\delta$  transition centered at 605 nm that is modestly blue-shifted with respect to experiment. Symmetry-breaking of the  $t_{2g}$  set of  $V^{2+}$  polypyridyls, which destabilizes the  $e_\delta$  orbitals, lowers the energy of the MLCT. The transitions centered at ~400 nm are MLCT bands that result in population of upper-lying  $\pi^*$ -orbitals: we suggest that the



**Figure 9.** Absorbance spectra of  $[V^{2+}(bpy)_3]$  as calculated by TD-DFT. For clarity, the  $NT\rho^{\alpha,\beta}$  of the MLCT absorbances are shown for the corresponding transition of  $[V^{2+}(bpy)(NH_3)_4]$ , noting that their energies are modestly red-shifted by  $\sim$ 400 cm $^{-1}$ .

symmetry-breaking trigonal distortion based on metal—ligand covalency leads to the increased intensity of the visible light absorbance for  $V^{2+}$  polypyridyls. We note that the  $^4(^3\mathrm{IL})$  of  $[V(bpy)(NH_3)_4]^{2+}$  described above is buried within this series of MLCT bands of greater intensity. This suggests that the  $^4(^3\mathrm{IL})$  is not an accessible pathway for intersystem crossing for  $V^{2+}$  polypyridyls. Our findings are consistent with the previous assignment of an MLCT transition as the pathway for intersystem crossing for  $V^{2+}$  polypyridyls.  $^{15}$ 

Table 1. Visible Absorbance Peaks,  $\lambda_{max}$  (nm), and Molar Absorptivities,  $\varepsilon$  (M<sup>-1</sup> cm<sup>-1</sup>), of the Complexes in the UV–Vis Spectra of Cr<sup>3+</sup> and V<sup>2+</sup> Polypyridyls

	visible absorbance peaks, $\lambda_{\max}$ (nm) $(\varepsilon)$
$ \begin{array}{c} [\operatorname{Cr}(\operatorname{bpy})_3](\operatorname{BF}_4)_3 \\ (\operatorname{Cr}1) \end{array} $	346 (8100), 360 (5680), 402 (950), 428 (682), 458 (291)
[Cr(phen) <sub>3</sub> ](BF <sub>4</sub> ) <sub>3</sub> (Cr2)	342 (6810), 358 (3710), 405 (821), 435 (558), 454 (285)
$ \begin{array}{c} [V(bpy)_3](OTf)_2 \\ (V1a) \end{array} $	404 (3460), 643 (5890)
[V(phen) <sub>3</sub> ](OTf) <sub>2</sub> (V2)	349 (3300), 640 (7980)

Assignment of Lowest Excited State. The change in spin density associated with the excitation from the  ${}^4A_2$  ground state  $(\rho_{4_A}^{\alpha,\beta})$  to the  ${}^2E$  excited state  $(\rho_{2_E}^{\alpha,\beta})$  of  $[Cr(bpy)_3]^{3+}$  is shown in the  $\Delta\rho^{\alpha,\beta}$  plot in Figure 10. The plot illustrates that one component of the  ${}^2E$  state is merely a spin flip within the nonbonding metal-centered,  $t_{2g}$ , orbital set relative to the ground state. This suggests minimal excited state geometric

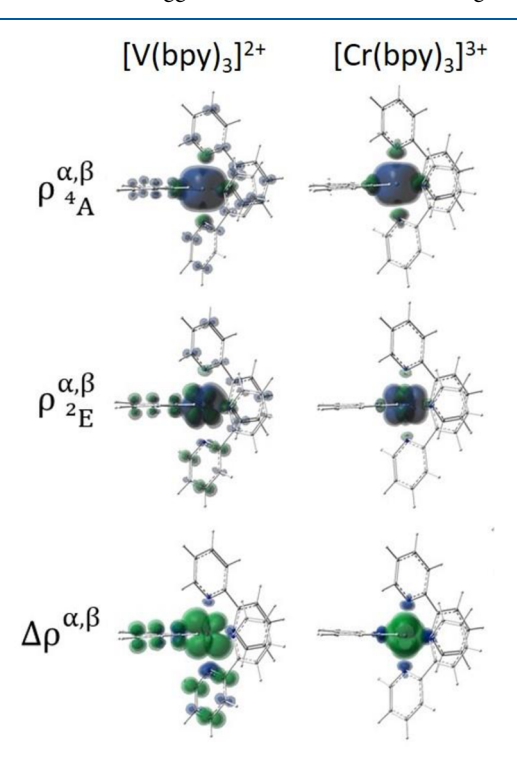


**Figure 10.** Spin density of the <sup>4</sup>A (top row) and <sup>2</sup>E state (middle row) of  $[Cr^{3+}(bpy)_3]$  (right column) and  $[V^{2+}(bpy)_3]$  (left column) where blue and green denote  $\alpha$  and  $\beta$  spin, respectively. The difference of the excited state with respect to the ground state,  $\Delta \rho^{\alpha,\beta}$  (bottom row) is presented below where green is associated with a  $\alpha \to \beta$  spin flip.

distortion and minimal nonradiative decay. We compute a  $^2$ E excitation energy of 1.62 eV (13100 cm $^{-1}$ ) using a multi-determinant approach to DFT further detailed in the Supporting Information, in agreement with the experimental value of 1.70 eV (13700 cm $^{-1}$ ). The optimized geometry of the  $^2$ E state confirms minimal distortion of the primary coordination sphere,  $\Delta S(\text{OC-6}) = 0.055$ . Collectively, the data suggest the excited state lifetime of Cr $^{3+}$  polypyridyls is attributable to minimal nonradiative decay of its spin-flip excited state.

While  $[V(bpy)_3]^{2^+}$  is nonemissive, as discussed above, the  $\Delta \rho^{\alpha,\beta}$  plot shows that the lowest energy transition, the spin flipped doublet, involves an  $e_\delta$  orbital. The transition is computed to occur at an energy of 1.10 eV (8870 cm<sup>-1</sup>), outside the range of our detectors. The plot also suggests that the  $[V^{2^+}(bpy)_3]$  E state is not entirely metal-centered, as the  $\beta \to \alpha$  spin flip delocalizes onto perpendicular pyridine groups, which is consistent with its greater trigonal distortion and metal-ligand covalency. The delocalization of the excited state reduces the overlap between the electron densities of the metal-centered orbitals, which in turn decreases the magnitude of its exchange interactions, lowering the energy of the Excited state. TD-DFT calculations indicate a broad and intense near-IR absorbance in the doublet manifold, which the NT $\rho^{\alpha,\beta}$  assigns as a  $\beta$ -transition of EMLCT character (Figure 11).

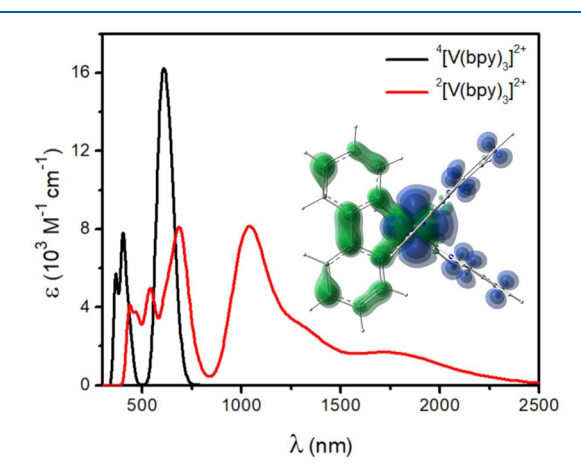


Figure 11. TD-DFT calculated absorbance of the quartet (black) and doublet (red) state of  $[V^{2+}(bpy)_3]$  and their energies with respect to the quartet ground state. The inset is the NT $\rho^{\alpha\beta}$  that corresponds to the third doublet excited state, with its energies and relevant properties included in the Supporting Information.

Previously, <sup>15</sup> some of us suggested that the lowest doublet state should be an admixture of the <sup>2</sup>E (<sup>2</sup>MC) and <sup>2</sup>MLCT states. These states should be near-degenerate and possess the same symmetry; coupling between them lowers the energy of the <sup>2</sup>MC state relative to a pure metal-centered <sup>2</sup>E excited state (Figure 12). This is further supported by the broadness of the transition.

In addition, the symmetry mixing associated with the observed trigonal distortion reported here also increases the ligand character of the  $V^{2+}$  <sup>2</sup>E state, which should also increase the coupling between the metal-centered doublet, <sup>2</sup>MC, and the lowest <sup>2</sup>MLCT states. This is functionally equivalent to suggesting an increase in covalency between the metal and ligand arises from the greater trigonal distortion of  $V^{2+}$ 

$$^{2}MC - ^{2}MLCT$$
 $^{2}MC \longrightarrow ^{2}MLCT$ 
 $^{2}MC + ^{2}MLCT$ 

**Figure 12.** Adiabatic coupling between doublet states of dominant metal character ( $^2$ E or  $^2$ MC) and the metal—ligand charge transfer ( $^2$ MLCT). This resonance results in a symmetric and antisymmetric combination of their states that splits their energies with respect to the average of their isolated states.

polypyridyls (see Figure 13). As suggested previously, the geometric distortion of the <sup>2</sup>MC/<sup>2</sup>MLCT state due to admixture of ligand character should facilitate intersystem crossing to the ground state and shorten the lifetime of the <sup>2</sup>MC/<sup>2</sup>MLCT state. <sup>15</sup>

We last consider the importance of the polypyridyl ligand environment. If the geometry of the quartet state is optimized for the series  $[V(bpy)_x(NH_3)_{6-2x}]^{2+}$ , where we sequentially substitute bipyridine with cis-coordinated amines, the trigonal distortion of the complex increases with the number of coordinated polypyridyls. We attribute this systematic distortion to metal—ligand  $\pi$ -covalency that is absent for NH<sub>3</sub>  $\sigma$ -donor ligands. In addition, we find an inverse relationship between the  $\varphi_{\text{OC} \to \text{TRP}}$  distortion and the calculated  $^2\text{E}$  excitation energy, as shown in Figure 14. This suggests that the trigonal distortion of  $V^{2+}$  polypyridyls is a result of metal—ligand  $\pi$ -interactions that concurrently stabilizes the  $^2\text{E}$  state.

# CONCLUSION

Rather than the analogous ground and excited state properties anticipated from the isoelectronic (d<sup>3</sup>) structure of Cr<sup>3+</sup> and V<sup>2+</sup> polypyridyl complexes, we report stark contrasts. The destabilized and expanded nature of the 3d orbitals of V2+ results in ligand  $\pi$ -metal  $t_{2g}$  orbital mixing and a pronounced trigonal distortion compared to the metal-ligand isolation and more rigorously octahedral coordination geometry of Cr3+ polypyridyls. This orbital mixing and trigonal geometric distortion delocalize the spin density of the paramagnetic metal center onto the ligand  $\pi^*$ -orbitals. Through DFT and multireference calculations, we find that the visible light absorbance of Cr3+ polypyridyl complexes results from a magnetic exchange interaction between the paramagnetic metal center and a ligand-centered triplet excited state. Because of the extensive metal-ligand charge transfer (MLCT) character of the quartet and doublet manifolds of  $V^{2+}$  polypyridyls, this pathway for intersystem crossing (ISC) is suppressed. Instead, significant delocalization of the <sup>2</sup>E state of the V<sup>2+</sup> complexes reduces the magnitude of its excitation

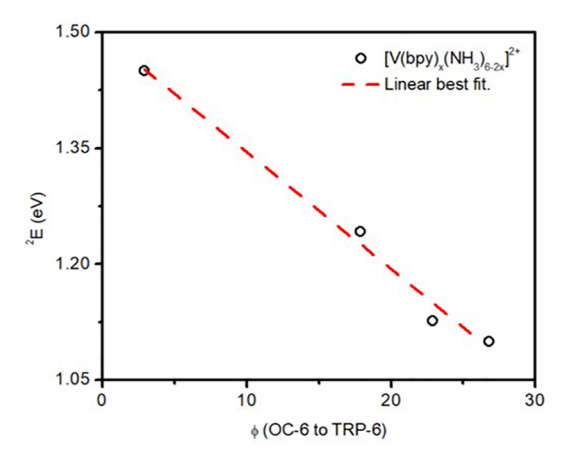


**Figure 14.** APFD multideterminant corrected  $^2E$  excitation energy of the  $[V(bpy)_x(NH_3)_{6-2x}]^{2+}$  as a function of the distortion pathway between octahedral and trigonal prismatic geometry.

energy that can be further stabilized by an adiabatic coupling with its near-degenerate  $^2$ MLCT state. Collectively, our findings complement the recent spectroscopic characterization of  $V^{2+}$  polypyridyls and provide context for its diminished excited state lifetimes compared to the robust photophysical properties of their  $Cr^{3+}$  analogues. In addition, they support an important emerging role for metal—ligand covalency in structural distortion and excited state tuning.

#### EXPERIMENTAL SECTION

**Preparation of Compounds.** All reactions were performed under either a nitrogen or an argon atmosphere at room temperature. The starting material  $[V(CH_3CN)_6](OTf)_2$  was prepared according to a previous literature report. Tetrabutylammonium hexafluorophosphate  $(Bu_4NPF_6)$  was recrystallized twice from ethanol before use. Ferrocene was sublimed before use. The syntheses of  $[Cr(bpy)_3](BF_4)_3$  (Cr1),  $[Cr(phen)_3](BF_4)_3$  (Cr2),  $[V(bpy)_3](OTf)_2$  (V1a),  $[V(bpy)_3](BPh_4)_2$  (V1b), and  $[V(phen)_3](OTf)_2$  (V2). have been reported previously.

[V(Me<sub>2</sub>bpy)<sub>3</sub>](OTf)<sub>2</sub> (V3). A solution of [V(CH<sub>3</sub>CN)<sub>6</sub>](OTf)<sub>2</sub> (41 mg, 0.069 mmol) and 4,4'-dimethyl-2,2'-bipyridine (38 mg, 0.206 mmol) in 5 mL of acetonitrile was stirred for 6 h at room temperature. The blue solution was dried *in vacuo* and washed with diethyl ether (3 × 3 mL). Diffusion of diethyl ether into a concentrated solution of the crude product in acetonitrile yielded 39 mg (0.043 mmol, 63% yield) of blue-plate crystals. UV-vis (CH<sub>2</sub>Cl<sub>2</sub>)  $\lambda_{\rm max}/{\rm nm}$  ( $\varepsilon_{\rm M}/{\rm M}^{-1}$  cm<sup>-1</sup>): 249 (29000), 298 (37600), 424 (3860), 659 (6300). IR (KBr pellet):  $\nu_{\rm C=N}$  1616 cm<sup>-1</sup>. ESI-MS(+) (CH<sub>3</sub>CN): m/z=301.83 (V3 - 2OTf<sup>-</sup>)<sup>2+</sup>. Anal. Calcd For C<sub>38</sub>H<sub>36</sub>F<sub>6</sub>N<sub>6</sub>O<sub>7</sub>S<sub>2</sub>V: C, 50.61; H, 4.02; N, 9.32. Found: C, 50.33; H, 4.21; N, 9.55.

 $[V(^tBu_2bpy)_3](OTf)_2$  (V4). A solution of  $[V(CH_3CN)_6](BPh_4)_2$  (95 mg, 0.102 mmol) and 4,4'-tert-2,2'-bipyridine (49 mg, 0.314 mmol) in 5 mL of acetonitrile was stirred for 6 h at room temperature. The

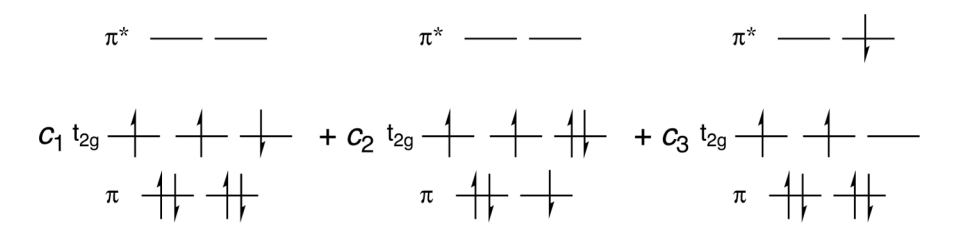


Figure 13. Symmetric linear combination of the singles excitations of  $(t_{2g} \leftarrow \pi)$  and  $(\pi^* \leftarrow t_{2g})$  character that are descriptive of greater metalligand covalency.

Scheme 1. General Synthesis of V(II) Polypyridyls

blue solution was dried *in vacuo* and washed with diethyl ether (3 × 3 mL). Diffusion of diethyl ether into a concentrated solution of the crude product in acetonitrile yielded 51 mg (0.044 mmol, 43% yield) of blue-plate crystals. UV–vis (CH<sub>3</sub>CN)  $\lambda_{\rm max}/{\rm nm}$  ( $\varepsilon_{\rm M}/{\rm M}^{-1}$  cm<sup>-1</sup>): 206 (119000), 296 (47500), 419 (5220), 652 (8240). IR (KBr pellet):  $\nu_{\rm C=N}$  1612 cm<sup>-1</sup>. ESI-MS(+) (CH<sub>3</sub>CN): m/z = 856.50 (V4 – 2OTf<sup>-</sup>)<sup>2+</sup>. Anal. Calcd For C<sub>78</sub>H<sub>64</sub>B<sub>2</sub>N<sub>6</sub>V: C, 58.27; H, 6.29; N, 7.28. Found: C, 57.95; H, 6.13; N, 7.18.

**Physical Methods.** Absorption spectra were cuvettes with a 1 cm path length, obtained with a Hewlett-Packard 8453 spectrometer in quartz. Voltammograms (Figure S18) were recorded with either a CH Instruments 1230A or Gamry Reference 600 potentiostat under a dinitrogen/argon atmosphere. All experiments used 0.1 M tetrabutyl-ammonium hexafluorophosphate (Bu<sub>4</sub>NPF<sub>6</sub>) solution in acetonitrile with a 0.25 mm Pt disk working electrode, Ag wire quasi-reference electrode, and a Pt wire auxiliary electrode. Reported potentials (Table S8) are referenced to the ferrocenium/ferrocene ([ $C_3H_5$ )<sub>2</sub>Fe]<sup>+</sup>/[( $C_5H_5$ )<sub>2</sub>Fe], Fc<sup>+/0</sup>) redox couple and were determined by adding ferrocene as an internal standard at the conclusion of each electrochemical experiment.

Crystallographic Measurements. For data collection, the crystal was coated in Paratone oil, supported on Cryoloops. V1b and V2 were mounted on a Bruker Kappa Apex II CCD and Bruker D8 Advance Quest diffractometer, respectively, under a stream of dinitrogen. Mo K $\alpha$  radiation and a graphite monochromator were used at 120 K for data collection. Initial lattice parameters were determined from reflections found in eight frames. Data sets were collected targeting complete coverage and 4-fold redundancy. Data were integrated and corrected for absorption effects with APEX 3 software. Structure were solved and refined with the SHELXTL software package. Unless noted otherwise, thermal parameters for all fully occupied, non-hydrogen atoms were refined anisotropically.

**Computational Procedures.** The  ${}^4A_2$  structures of the [Cr-(PDO)<sub>3</sub>]<sup>3+</sup> and [V(PDO)<sub>3</sub>]<sup>2+</sup> complexes (PDO is 1,3-propanedionate) were optimized with the APFD functional<sup>52</sup> and the cc-pVTZ basis set<sup>53</sup> by using the Gaussian09 software package.<sup>54</sup> The structure for the  ${}^4A_2$  ground state was also used to represent the  ${}^2E$  state. The  ${}^4T_2$  excited state structures were calculated by promoting an electron from the  ${}^4L_2$  orbital to an  ${}^8E_3$  orbital, its geometry constrained as  ${}^8E_2$ -symmetric. The excited state was further optimized without the symmetry restriction resulting in the vibrational minimum structure that we define as  ${}^4L_2$ . A linearly interpolated path between the  ${}^8E_3$  and  ${}^4L_3$  states was obtained following the method of Miller et al.  ${}^{55}$ 

The excited state energies for the interpolated path structures were calculated with the SORCI method with a CAS(3,5) zeroth-order wave function. <sup>24</sup> The cc-pCVTZ<sup>56</sup> and cc-pVDZ basis sets were used for the metal center and the remaining atoms, respectively. The active space of the SORCI calculation was expanded to include the metal-center 3p orbitals. Spin—orbit coupling was calculated for structures

within the 0.50–0.75 range of the distortion pathway. All SORCI related calculations were performed by using the ORCA electronic structure software package (ver. 3.0.3).<sup>57</sup>

The ground state ( ${}^{4}$ A) structures of compounds [ $M^{n+}(4,4'-X-bpy)_{3}$ ] ( $M = Cr^{3+}$  and  $V^{2+}$ ; X = H,  $CH_{3}$ , tert-butyl,  $CF_{3}$ , and  $CO_{2}Me$ ) were optimized by using DFT with the APFD functional and the 6-311+G\* basis set<sup>58</sup> in a PCM acetonitrile continuum solvent.<sup>59</sup> An analogous procedure was used for the optimization of the model complexes  $[Cr(NH_3)_4(bpy)]^{3+}$  and  $[V(bpy)_x(NH_3)_{6-2x}]^{2+}$ . All DFT calculations utilized the Gaussian 16 software suite. 60 An unrestricted wave function was used coupled with a stability analysis to verify the wave function as the lowest of a given  $M_s$ . The geometries for the  ${}^2\mathrm{E}$ excited state of [Cr(bpy)<sub>3</sub>]<sup>3+</sup> and [V(bpy)<sub>3</sub>]<sup>2+</sup> were optimized as well about their stable wave function. TD-DFT calculations<sup>61</sup> and natural transition orbital (NTO)<sup>62</sup> and natural transition spin density  $(\mathrm{NT}
ho^{lpha,eta})$  analyses were performed on the quartet and doublet state of the Cr<sup>3+</sup> and V<sup>2+</sup> polypyridyl complexes. The electronic absorption spectra were generated by using the oscillator strengths and peak positions from the corresponding TD-DFT calculation. Each electronic state was convoluted with a Gaussian line shape with a 0.219 eV line width.

The following calculations were performed with the ORCA 4.0 electronic structure software program.  $^{63}$  The molecular orbitals and qualitative energies presented in Figures 2 and 3 were generated with the B3LYP functional  $^{64}$  and the def2-TZVP basis set  $^{65}$  and the previously detailed D3(Ar2) empirical dispersion correction.  $^{64}$  The spin determinants of the CAS(5,7) wave function of [Cr(bpy)-(NH3)4]^3+ and [V(bpy)(NH3)4]^2+ were determined with the def2-TZVP basis set and the corresponding auxiliary basis sets. The active space was defined as the metal-centered  $\rm t_{2g}$  and  $\rm e_g^*$  orbitals and the ligand-based  $\pi$  and  $\pi^*$  orbitals. The final energies for the excited states were obtained with the NEVPT2(5,7) technique.  $^{49,66,67}$ 

The vibronic spectrum of  $[Cr(bpy)(NH_3)_4]^{3+}$  was calculated with the APFD functional and 6-311+g(d) basis set with the Gaussian16 software. The geometry of the lowest-lying quartet excited state via TD-DFT was optimized. Frequency calculations of the ground and the corresponding excited states were performed. As previously described by Santoro et al., the vibronic spectrum was generated by Franck–Condon–Herzberg–Teller analysis for a one-photon absorption between the ground and excited state. 68

### ASSOCIATED CONTENT

### Supporting Information

The Supporting Information is available free of charge at https://pubs.acs.org/doi/10.1021/acs.inorgchem.1c01129.

Crystal structure details, electrochemistry, structural analysis, substituent impact, TD-DFT, natural transition spin density  $(NT\rho^{\alpha,\beta})$ , multireference DFT correction,

qualitative orbital energy diagrams, Franck–Condon–Herzberg–Teller analysis of  ${}^{4}[{}^{3}(IL)]$ , spin determinants of  ${}^{4}[{}^{3}(IL)]$  (PDF)

#### **Accession Codes**

CCDC 2077089–2077090 contain the supplementary crystallographic data for this paper. These data can be obtained free of charge via www.ccdc.cam.ac.uk/data\_request/cif, or by emailing data\_request@ccdc.cam.ac.uk, or by contacting The Cambridge Crystallographic Data Centre, 12 Union Road, Cambridge CB2 1EZ, UK; fax: +44 1223 336033.

#### AUTHOR INFORMATION

## **Corresponding Authors**

Anthony K. Rappé – Department of Chemistry, Colorado State University, Fort Collins, Colorado 80523, United States; © orcid.org/0000-0002-5259-1186;

Email: anthony.rappe@colostate.edu

Matthew P. Shores – Department of Chemistry, Colorado State University, Fort Collins, Colorado 80523, United States; © orcid.org/0000-0002-9751-0490;

Email: matthew.shores@colostate.edu

#### **Authors**

Justin P. Joyce – Department of Chemistry, Colorado State University, Fort Collins, Colorado 80523, United States; orcid.org/0000-0002-8287-622X

Romeo I. Portillo – Department of Chemistry, Colorado State University, Fort Collins, Colorado 80523, United States

Collette M. Nite – Department of Chemistry, Colorado State University, Fort Collins, Colorado 80523, United States

Jacob M. Nite – Department of Chemistry, Colorado State University, Fort Collins, Colorado 80523, United States; orcid.org/0000-0001-7425-6795

Michael P. Nguyen – Department of Chemistry, Colorado State University, Fort Collins, Colorado 80523, United States

Complete contact information is available at: https://pubs.acs.org/10.1021/acs.inorgchem.1c01129

# **Author Contributions**

<sup>†</sup>J.P.J. and R.I.P. contributed equally to this work and are cofirst authors.

# Notes

The authors declare no competing financial interest.

## ACKNOWLEDGMENTS

This work was performed by the Catalysis Collaboratory for Light-activated Earth Abundant Reagents (C-CLEAR), which was supported by the National Science Foundation and the Environmental Protection Agency through the Networks for Sustainable Molecular Design and Synthesis (NSF-CHE-1339674). Support from NSF-CHE-1956399 is also acknowledged.

## REFERENCES

- (1) Wenger, O. S. Photoactive Complexes with Earth-Abundant Metals. J. Am. Chem. Soc. 2018, 140 (42), 13522–13533.
- (2) Förster, C.; Heinze, K. Photophysics and Photochemistry with Earth-Abundant Metals Fundamentals and Concepts. *Chem. Soc. Rev.* **2020**, 49 (4), 1057–1070.
- (3) Sugano, S.; Tsujikawa, I. Absorption Spectra of Cr3 in A1203 Part B. Experimental Studies of the Zeeman Effect and Other

Properties of the Line Spectra. J. Phys. Soc. Jpn. 1958, 13 (8), 899–910.

- (4) Sugano, S.; Tanabe, Y. Absorption Spectra of Cr3+ in A1203 Part A. Theoretical Studies of the Absorption Bands and Lines. *J. Phys. Soc. Jpn.* **1958**, *13* (8), 880–899.
- (5) Finkelstein, R.; Van Vleck, J. H. On the Energy Levels of Chrome Alum. J. Chem. Phys. 1940, 8 (10), 790-797.
- (6) Singh, S. K.; Eng, J.; Atanasov, M.; Neese, F. Covalency and Chemical Bonding in Transition Metal Complexes: An Ab Initio Based Ligand Field Perspective. *Coord. Chem. Rev.* **2017**, 344, 2–25.
- (7) Kirk, A. D. Photochemistry and Photophysics of Chromium(III) Complexes. *Chem. Rev.* **1999**, *99*, 1607–1640.
- (8) Jørgensen, C. K. Spectroscopy of Transition-Group Complexes. *Adv. Chem. Phys.* **2007**, *5*, 33–146.
- (9) Forster, L. S. Thermal Relaxation in Excited Electronic States of D3 and D6Metal Complexes. *Coord. Chem. Rev.* **2002**, 227, 59–92.
- (10) Lever, A. B. P. In *Inorganic Electronic Spectroscopy*, 2nd ed.; Elsevier: Amsterdam, 1984; p 126.
- (11) König, E.; Herzog, S. Electronic Spectra of Tris(2,2'-Bipyridyl) Complexes—II. *J. Inorg. Nucl. Chem.* **1970**, 32 (2), 601–611.
- (12) König, E.; Herzog, S. Electronic Spectra of Tris(2,2'-Bipyridyl) Complexes—I. *J. Inorg. Nucl. Chem.* **1970**, 32 (2), 585–599.
- (13) Shah, S. S.; Maverick, A. W. Photophysics and Photochemistry of 2,2'-Bipyridine and 1,10-Phenanthroline Complexes of Vanadium-(II). *Inorg. Chem.* **1986**, 25 (11), 1867–1871.
- (14) Maverick, A. W.; Shah, S. S.; Kirmaier, C.; Holten, D. Nature of the Lowest Energy Excited State in Vanadium(II) Polypyridine Complexes. *Inorg. Chem.* **1987**, *26* (5), 774–776.
- (15) Dill, R. D.; Portillo, R. I.; Shepard, S. G.; Shores, M. P.; Rappé, A. K.; Damrauer, N. H. Long-Lived Mixed 2 MLCT/MC States in Antiferromagnetically Coupled d 3 Vanadium(II) Bipyridine and Phenanthroline Complexes. *Inorg. Chem.* **2020**, *59* (20), 14706–14715.
- (16) Görbitz, C. H. The Development and Use of a Crystallographic Database. *Acta Crystallogr., Sect. B: Struct. Sci., Cryst. Eng. Mater.* **2016**, 72 (2), 167–168.
- (17) Cordero, B.; Gómez, V.; Platero-Prats, A. E.; Revés, M.; Echeverría, J.; Cremades, E.; Barragán, F.; Alvarez, S. Covalent Radii Revisited. *J. Chem. Soc. Dalt. Trans.* **2008**, *21*, 2832–2838.
- (18) Taylor, M. G.; Yang, T.; Lin, S.; Nandy, A.; Janet, J. P.; Duan, C.; Kulik, H. J. Seeing Is Believing: Experimental Spin States from Machine Learning Model Structure Predictions. *J. Phys. Chem. A* **2020**, *124* (16), 3286–3299.
- (19) Casanova, D.; Cirera, J.; Llunell, M.; Alemany, P.; Avnir, D.; Alvarez, S. Minimal Distortion Pathways in Polyhedral Rearrangements. J. Am. Chem. Soc. 2004, 126 (6), 1755–1763.
- (20) Bailar, J. C. Some Problems in the Stereochemistry of Coordination Compounds. *J. Inorg. Nucl. Chem.* **1958**, 8 (C), 165–175.
- (21) Cremades, E.; Echeverría, J.; Alvarez, S. The Trigonal Prism in Coordination Chemistry. *Chem. Eur. J.* **2010**, *16* (34), 10380–10396
- (22) Kranida, A.; Ralchenko, Y.; Reader, J.; Team, N. A. NIST Atomic Spectra Database.
- (23) Maestri, M.; Bolletta, F.; Moggi, L.; Balzani, V.; Henry, M. S.; Hoffman, M. Z. Photochemistry and Photophysics of Tris(2,2'-Bipyridine)Chromium(III). *J. Chem. Soc., Chem. Commun.* 1977, 14, 491–492.
- (24) Neese, F. A Spectroscopy Oriented Configuration Interaction Procedure. J. Chem. Phys. 2003, 119 (18), 9428-9443.
- (25) Nite, J. M. Spin Multiplets: Theory and Application, Colorado State University, 2018.
- (26) Juban, E. A.; McCusker, J. K. Ultrafast Dynamics of 2E State Formation in Cr(Acac)3. *J. Am. Chem. Soc.* **2005**, 127 (18), 6857–6865.
- (27) Juban, E. A.; Smeigh, A. L.; Monat, J. E.; McCusker, J. K. Ultrafast Dynamics of Ligand-Field Excited States. *Coord. Chem. Rev.* **2006**, 250, 1783–1791.

- (28) Ando, H.; Iuchi, S.; Sato, H. Theoretical Study on Ultrafast Intersystem Crossing of Chromium(III) Acetylacetonate. *Chem. Phys. Lett.* **2012**, 535, 177–181.
- (29) Higgins, R. F.; Fatur, S. M.; Shepard, S. G.; Stevenson, S. M.; Boston, D. J.; Ferreira, E. M.; Damrauer, N. H.; Rappé, A. K.; Shores, M. P. Uncovering the Roles of Oxygen in Cr(III) Photoredox Catalysis. *J. Am. Chem. Soc.* **2016**, *138* (16), 5451–5464.
- (30) Atanasov, M.; Schönherr, T. The Role of  $\pi$ -Bonding for Trigonal Level Splittings in Chelate Complexes. 3. The Lowest Electronic States in Cr(Acac)3. *Inorg. Chem.* **1990**, 29 (22), 4545–4550.
- (31) Schönherr, T.; Atanasov, M.; Hauser, A. Role of  $\pi$ -Bonding for Trigonal Level Splittings in Chromium(III) Complexes. 4. Doublet States and Zeeman Level Splittings in [Cr(Bpy)3]3+. *Inorg. Chem.* **1996**, 35 (7), 2077–2084.
- (32) Hancock, R. D.; McDougall, G. J. The Role of Electronic Delocalization over the Chelate Ring in Stabilizing Complexes of 2,2′-Bipyridyl. *J. Chem. Soc., Dalton Trans.* **1977**, *1*, 67–70.
- (33) Josephsen, J.; Schäffer, C. E.; Ratkje, S. K.; Pouchard, M.; Hagenmuller, P.; Andresen, A. F. The Position of 2,2'-Bipyridine and 1,10-Phenanthroline in the Spectrochemical Series. *Acta Chem. Scand.* 1977, 31a, 813–824.
- (34) Doistau, B.; Collet, G.; Bolomey, E. A.; Sadat-Noorbakhsh, V.; Besnard, C.; Piguet, C. Heteroleptic Ter-Bidentate Cr(III) Complexes as Tunable Optical Sensitizers. *Inorg. Chem.* **2018**, *57* (22), 14362–14373.
- (35) Otto, S.; Grabolle, M.; Förster, C.; Kreitner, C.; Resch-Genger, U.; Heinze, K. [Cr(Ddpd)2]3+: A Molecular, Water-Soluble, Highly NIR-Emissive Ruby Analogue. *Angew. Chem., Int. Ed.* **2015**, *54* (39), 11572–11576.
- (36) Jiménez, J. R.; Doistau, B.; Besnard, C.; Piguet, C. Versatile Heteroleptic Bis-Terdentate Cr(Iii) Chromophores Displaying Room Temperature Millisecond Excited State Lifetimes. *Chem. Commun.* **2018**, *54* (94), 13228–13231.
- (37) Treiling, S.; Wang, C.; Förster, C.; Reichenauer, F.; Kalmbach, J.; Boden, P.; Harris, J. P.; Carrella, L. M.; Rentschler, E.; Resch-Genger, U.; Reber, C.; Seitz, M.; Gerhards, M.; Heinze, K. Luminescence and Light-Driven Energy and Electron Transfer from an Exceptionally Long-Lived Excited State of a Non-Innocent Chromium(III) Complex. Angew. Chem., Int. Ed. 2019, 58 (50), 18075—18085.
- (38) Ashley, D. C.; Jakubikova, E. Tuning the Redox Potentials and Ligand Field Strength of Fe(II) Polypyridines: The Dual  $\pi$ -Donor and  $\pi$ -Acceptor Character of Bipyridine. *Inorg. Chem.* **2018**, *57* (16), 9907–9917
- (39) Mukherjee, S.; Torres, D. E.; Jakubikova, E. HOMO Inversion as a Strategy for Improving the Light-Absorption Properties of Fe(II) Chromophores. *Chem. Sci.* **2017**, *8* (12), 8115–8126.
- (40) Dobson, J. C.; Taube, H. Coordination Chemistry and Redox Properties of Polypyridyl Complexes of Vanadium (II). *Inorg. Chem.* **1989**, 28 (7), 1310–1315.
- (41) McDaniel, A. M.; Tseng, H. W.; Damrauer, N. H.; Shores, M. P. Synthesis and Solution Phase Characterization of Strongly Photooxidizing Heteroleptic Cr(III) Tris-Dipyridyl Complexes. *Inorg. Chem.* **2010**, *49* (17), 7981–7991.
- (42) Jiménez, J. R.; Poncet, M.; Doistau, B.; Besnard, C.; Piguet, C. Luminescent Polypyridyl Heteroleptic CrIIIcomplexes with High Quantum Yields and Long Excited State Lifetimes. *Dalt. Trans.* **2020**, 49 (39), 13528–13532.
- (43) Barbour, J. C.; Kim, A. J. I.; DeVries, E.; Shaner, S. E.; Lovaasen, B. M. Chromium(III) Bis-Arylterpyridyl Complexes with Enhanced Visible Absorption via Incorporation of Intraligand Charge-Transfer Transitions. *Inorg. Chem.* **2017**, *56* (14), 8212–8222.
- (44) Ohno, T.; Kato, S.; Kaizaki, S.; Hanazaki, I. Singlet-Triplet Transitions of Aromatic Compounds Coordinating to a Paramagnetic Chromium(III) Ion. *Inorg. Chem.* **1986**, 25 (22), 3853–3858.
- (45) Noodleman, L.; Davidson, E. R. Ligand Spin Polarization and Antiferromagnetic Coupling in Transition Metal Dimers. *Chem. Phys.* **1986**, *109* (1), 131–143.

- (46) Noodleman, L. Valence Bond Description of Antiferromagnetic Coupling in Transition Metal Dimers. *J. Chem. Phys.* **1981**, *74* (10), 5737–5743.
- (47) Angeli, C.; Cimiraglia, R.; Evangelisti, S.; Leininger, T.; Malrieu, J. P. Introduction of N-Electron Valence States for Multireference Perturbation Theory. *J. Chem. Phys.* **2001**, *114* (23), 10252.
- (48) Angeli, C.; Cimiraglia, R.; Malrieu, J. P. N-Electron Valence State Perturbation Theory: A Fast Implementation of the Strongly Contracted Variant. *Chem. Phys. Lett.* **2001**, *350* (3–4), 297–305.
- (49) Angeli, C.; Cimiraglia, R.; Malrieu, J. P. N-Electron Valence State Perturbation Theory: A Spinless Formulation and an Efficient Implementation of the Strongly Contracted and of the Partially Contracted Variants. *J. Chem. Phys.* **2002**, *117* (20), 9138–9153.
- (50) Bechlars, B.; D'Alessandro, D. M.; Jenkins, D. M.; Iavarone, A. T.; Glover, S. D.; Kubiak, C. P.; Long, J. R. High-Spin Ground States via Electron Delocalization in Mixed-Valence Imidazolate-Bridged Divanadium Complexes. *Nat. Chem.* **2010**, *2* (5), 362–368.
- (51) Higgins, R. F.; Fatur, S. M.; Damrauer, N. H.; Ferreira, E. M.; Rappé, A. K.; Shores, M. P. Detection of an Energy-Transfer Pathway in Cr-Photoredox Catalysis. *ACS Catal.* **2018**, 8 (10), 9216–9225.
- (52) Austin, A.; Petersson, G. A.; Frisch, M. J.; Dobek, F. J.; Scalmani, G.; Throssell, K. A Density Functional with Spherical Atom Dispersion Terms. *J. Chem. Theory Comput.* **2012**, *8*, 4989–5007.
- (53) Woon, D. E.; Dunning, T. H. Gaussian Basis Sets for Use in Correlated Molecular Calculations. V. Core-Valence Basis Sets for Boron through Neon. *J. Chem. Phys.* **1995**, *103*, 4572–4585.
- (54) Frisch, M. J.; Trucks, G. W.; Schlegel, H. B.; Scuseria, G. E.; Robb, M. A.; Cheeseman, J. R.; Scalmani, G.; Barone, V.; Petersson, G. A.; Nakatsuji, H.; Li, X.; Caricato, M.; Marenich, A.; Bloino, J.; Janesko, B. G.; Gomperts, R.; Mennucci, B.; Hratchian, H. P.; Ortiz, J. V.; et al. *Gaussian 09*, Rev. D.01; Gaussian, Inc.: Wallingford, CT, 2009.
- (55) Miller, W. H.; Ruf, B. A.; Chang, Y. T. A Diabatic Reaction Path Hamiltonian. *J. Chem. Phys.* **1988**, 89 (10), 6298–6304.
- (56) Rappoport, D.; Furche, F. Property-Optimized Gaussian Basis Sets for Molecular Response Calculations. *J. Chem. Phys.* **2010**, *133* (13), 134105.
- (57) Neese, F. The ORCA Program System. Wiley Interdiscip. Rev.: Comput. Mol. Sci. 2012, 2 (1), 73–78.
- (58) Krishnan, R.; Binkley, J. S.; Seeger, R.; Pople, J. A. Self-Consistent Molecular Orbital Methods. XX. A Basis Set for Correlated Wave Functions. J. Chem. Phys. 1980, 72 (1), 650–654.
- (59) Tomasi, J.; Mennucci, B.; Cammi, R. Quantum Mechanical Continuum Solvation Models. Chem. Rev. 2005, 105 (8), 2999–3093.
- (60) Frisch, M. J.; Trucks, G. W.; Schlegel, H. B.; Scuseria, G. E.; Robb, M. A.; Cheeseman, J. R.; Scalmani, G.; Barone, V.; Petersson, G. A.; Nakatsuji, H.; Li, X.; Caricato, M.; Marenich, A. V.; Bloino, J.; Janesko, B. G.; Gomperts, R.; Mennucci, B.; Hratchian, H. P.; et al. *Gaussian* 16, Rev. B.01; Gaussian, Inc..: Wallingford, CT, 2016.
- (61) Stratmann, R. E.; Scuseria, G. E.; Frisch, M. J. An Efficient Implementation of Time-Dependent Density-Functional Theory for the Calculation of Excitation Energies of Large Molecules. *J. Chem. Phys.* **1998**, *109* (19), 8218–8224.
- (62) Martin, R. L. Natural Transition Orbitals. J. Chem. Phys. 2003, 118 (11), 4775–4777.
- (63) Neese, F. Software Update: The ORCA Program System. Wiley Interdiscip. Rev.: Comput. Mol. Sci. 2018, DOI: 10.1002/wcms.1327.
- (64) Becke, A. D. Density-Functional Thermochemistry. III. The Role of Exact Exchange. J. Chem. Phys. 1993, 98 (7), 5648–5652.
- (65) Weigend, F.; Ahlrichs, R. Balanced Basis Sets of Split Valence, Triple Zeta Valence and Quadruple Zeta Valence Quality for H to Rn: Design and Assessment of Accuracy. *Phys. Chem. Chem. Phys.* **2005**, 7 (18), 3297–3305.
- (66) Angeli, C.; Cimiraglia, R.; Evangelisti, S.; Leininger, T.; Malrieu, J. P. Introduction of N-Electron Valence States for Multireference Perturbation Theory. *J. Chem. Phys.* **2001**, *114* (23), 10252.

(67) Angeli, C.; Pastore, M.; Cimiraglia, R. New Perspectives in Multireference Perturbation Theory: The n-Electron Valence State Approach. *Theor. Chem. Acc.* **2007**, *117* (5–6), 743–754.

(68) Santoro, F.; Lami, A.; Improta, R.; Bloino, J.; Barone, V. Effective Method for the Computation of Optical Spectra of Large Molecules at Finite Temperature Including the Duschinsky and Herzberg-Teller Effect: The Qx Band of Porphyrin as a Case Study. *J. Chem. Phys.* **2008**, *128* (22), 224311.